Materials Today Bio 15 (2022) 100310

Contents lists available at ScienceDirect

Materials Today Bio

journal homepage: www.journals.elsevier.com/materials-today-bio

Acellular cartilage matrix biomimetic scaffold with immediate enrichment of autologous bone marrow mononuclear cells to repair articular cartilage defects

Litao Jia [a,b,c,1], Peiling Zhang [a,1], Zheng Ci [a,c,1], Xiaoyan Hao [d], Baoshuai Bai [c], Wei Zhang [a,c], Haiyue Jiang [b,**], Guangdong Zhou [a,c,*]

[a] Department of Plastic and Reconstructive Surgery, Shanghai Key Laboratory of Tissue Engineering, Shanghai Ninth People's Hospital, Shanghai Jiao Tong University School of Medicine, Shanghai, 200011, PR China
[b] Research Center of Plastic Surgery Hospital, Chinese Academy of Medical Sciences and Peking Union Medical College, Beijing, 100144, PR China
[c] Research Institute of Plastic Surgery, Weifang Medical University, Weifang, 261042, PR China
[d] Department of Cosmetology and Plastic Surgery, The First Affiliated Hospital of Weifang Medical University, Weifang, Shandong, 261000, PR China

ARTICLE INFO

Keywords:
Acellular cartilage matrix
Biomimetic scaffold
Bone marrow mononuclear cells
Density gradient centrifugation
Articular cartilage repair

ABSTRACT

Functional repair of articular cartilage defects is always a great challenge in joint surgery clinically. Tissue engineering strategies that combine autologous cell implantation with three-dimensional scaffolds have proven effective for repairing articular cartilage tissue. However, it faces the problem of cell sources and scaffold materials. Autologous chondrocytes and bone marrow are difficult to popularize clinically due to limited donor sources and low mononuclear cell (MNC) concentrations, respectively. The density gradient centrifugation method can increase the concentration of MNCs in fresh bone marrow by nearly a hundredfold and achieve immediate enrichment. In addition, acellular cartilage matrix (ACM), with good biocompatibility and a cartilage-specific microenvironment, is considered to be an ideal candidate scaffold for cartilage regeneration. In this study, hybrid pigs were used to establish articular cartilage defect models of different sizes to determine the feasibility and maximum scope of application of ACM-based biomimetic scaffolds combined with MNCs for inducing articular cartilage regeneration. Importantly, ACM-based biomimetic scaffolds instantly enriched MNCs could improve the repair effect of articular cartilage defects *in situ*, which established a new model of articular cartilage regeneration that could be applied immediately and suited for large-scale clinical promotion. The current study significantly improves the repair effect of articular cartilage defects, which provides scientific evidence and detailed insights for future clinical applications of ACM-based biomimetic scaffolds combined with MNCs.

1. Introduction

Functional repair of articular cartilage defects is always a great challenge in joint surgery clinically because of the poor self-repair capability [1,2]. The current methodology used for repairing articular cartilage defects includes abrasion arthroplasty, microfractures, and autologous cartilage transplantation, but the overall therapeutic effect is unsatisfactory and lacks ideal donor sources [3–6]. Therefore, how to achieve articular cartilage regeneration and functional reconstruction is still an urgent problem to be solved. Over the past 20 years, tissue engineering strategies that combine autologous chondrocyte or stem cell implantation with three-dimensional (3D) scaffolds have proven effective for regenerating cartilage tissues [7–9]. However, strategies using autologous chondrocytes as the cell sources will inevitably be associated with a limited supply of cells and donor site morbidity. Autologous bone marrow mononuclear cells (BMMNCs) could overcome the above problem of cell sources [10,11]. Unfortunately, fresh bone marrow with an extremely low concentration of mononuclear cells (MNCs) is not suitable

* Corresponding author. Department of Plastic and Reconstructive Surgery, Shanghai Key Laboratory of Tissue Engineering, Shanghai Ninth People's Hospital, Shanghai Jiao Tong University School of Medicine, Shanghai, 200011, PR China.
** Corresponding author. Research Center of Plastic Surgery Hospital, Chinese Academy of Medical Sciences and Peking Union Medical College, Beijing 100144, P.R. China.
E-mail addresses: jianghaiyue@psh.pumc.edu.cn (H. Jiang), guangdongzhou@126.com (G. Zhou).
[1] These authors contributed equally to this work.

https://doi.org/10.1016/j.mtbio.2022.100310
Received 18 March 2022; Received in revised form 13 May 2022; Accepted 26 May 2022
Available online 28 May 2022

for immediate enrichment, and cell isolation and proliferation require additional culture time *in vitro* [12,13], which makes it difficult to achieve immediate enrichment of cells and tissue repair. Therefore, it is difficult to achieve further clinical application.

To realize immediate enrichment, MNCs could be isolated instantly from fresh bone marrow by density gradient centrifugation [14], in which the concentration of MNCs could be increased nearly a hundred-fold. Noteworthily, biological scaffolds also play an important role in tissue engineering [15,16]. Therefore, a proper scaffold with good biocompatibility is urgently required to assist in cartilage regeneration. Among all scaffolds, acellular cartilage matrix (ACM) with good biocompatibility, containing a cartilage-specific microenvironment and bioactive factors, is considered to be one of the ideal candidate scaffolds for cartilage regeneration [17–20].

In the current study, hybrid pigs, whose knee joints were relatively similar to those of humans in structure and load-bearing conditions, were used to establish articular cartilage defect models of different sizes in diameter to clarify the feasibility and maximum scope of application of ACM-based biomimetic scaffolds for inducing articular cartilage regeneration. Most importantly, the ACM-based biomimetic scaffold instantly enriched MNCs to explore whether it could improve the repair effect of articular cartilage defects *in situ* and the maximum scope of application. The current study provides scientific evidence and detailed insights for future clinical application of ACM-based biomimetic scaffolds and instant enrichment of MNCs to repair articular cartilage defects.

2. Materials and methods

2.1. Materials and animals

All chemicals were reagent grade and supplied by Sigma–Aldrich (St. Louis, USA) unless otherwise stated. Eighteen hybrid pigs (10 males and 8 females, 4 months old) were purchased from Shanghai Jiagan Biological Technology Co. (Shanghai, China). All protocols for experimenting on animals were approved by the Animal Care and Experiment Committee of Shanghai Jiaotong University School of Medicine (Shanghai, China).

2.2. Preparation of scaffolds

Gelatin (GT) scaffolds and ACM/GT scaffolds were prepared according to our previously reported protocols [18,21]. Briefly, ACM powder was prepared after freeze-grinding and decellularization procedures. Then, the specific concentration and proportion of ACM suspension and gelatin solution (2% concentrations, ACM: GT = 5: 5) that were optimized in the previous experiment were blended and freeze-dried to fabricate porous ACM/GT scaffolds. Similarly, gelatin solution at a 2% concentration was freeze-dried to fabricate porous GT scaffolds. The ACM/GT and GT suspensions were separately poured into cylindrical silicone molds and then freeze-dried to fabricate three-dimensional porous ACM/GT and GT scaffolds. To improve the stability of these scaffolds, they were crosslinked using 1-ethyl-3-(3-dimethylaminopropyl) carbodiimide (EDC)/N-hydroxysuccinimide (NHS) (EDC and NHS dissolved in 98% ethanol, 5% and 3% in EDC and NHS, respectively) for 24 h, then lyophilized again and sterilized with ethylene oxide before use.

2.3. Proteomic analysis of scaffolds

The ACM and native cartilage samples were dissolved and cracked to extract protein for proteomic analysis using a Q Exactive™ LC-MS/MS system (Thermo Fisher Scientific) as described previously. The MS spectra were searched against the UniProt *Sus scrofa* reference proteome FASTA file using Protein Discover 2.2 software. A decoy database containing reverse sequences of the proteins was also used. The resultant peptides were assembled into protein groups, and only proteins with at least two distinct peptides were considered reliable. The proteins preserved and lost in ACM after decellularization was screened out respectively. And a hypergeometric test was used to perform Gene Ontology (GO) analysis on the identified proteins to determine the biological functions of the preserved and lost proteins.

2.4. Characterization of scaffolds

2.4.1. Morphological analysis of scaffolds

The morphology of the ACM/GT scaffolds and GT scaffolds was observed using scanning electron microscopy (SEM, Philips XL-30, Amsterdam, Netherlands) at an accelerating voltage of 15 kV. The average pore size of ACM/GT scaffolds and GT scaffolds was analyzed by measuring at least 100 random pores in the SEM images using ImageJ software.

2.4.2. Porosity analysis of scaffolds

The porosity of the ACM/GT scaffolds and GT scaffolds was tested using the ethanol infiltration method as described in a previous study [22]. Briefly, V_1 and V_2 were set as the volume of ethanol in the measuring bottle before and after the scaffolds were immersed in ethanol, respectively. The V_3 was marked as the remaining volume in which the scaffold was removed from the ethanol after 15 min. Then, the porosity of the ACM/GT scaffolds and GT scaffolds (n = 5 per group) was calculated using the following formula:

$$Porosity\ (\%) = \frac{V_1 - V_3}{V_2 - V_3} \times 100\%$$

2.4.3. Mechanical analysis of scaffolds

The mechanical properties of ACM/GT scaffolds and GT scaffolds were determined using a mechanical testing machine (Instron-5542, Canton, MA) as described in previously reported methods [23]. Briefly, ACM/GT scaffolds and GT scaffolds (n = 5 per group) were processed to a cylindrical shape via refinement, and then a constant compressive strain rate of 0.5 mm/min was applied until 80% of the maximal deformation. The Young's modulus for each of the tested samples was then calculated based on the slope of the stress-strain curve.

2.5. Biocompatibility of scaffolds

2.5.1. Cell seeding efficiency

Bone marrow was aspirated from the anterior superior iliac spine of one hybrid pig under anesthetic and disinfection conditions. Bone marrow mesenchymal stem cells (BMSCs) were isolated, cultured, and expanded according to previously established methods [24]. BMSCs from passage 2 were adjusted to a final concentration of 20×10^6 cells/mL and 150 μL cell suspension was seeded into ACM/GT scaffolds and GT scaffolds (recorded as total cell number, N_t). After 24 h of incubation, the remaining cells (N_r) were collected and counted, and then the cell seeding efficiencies for each scaffold were calculated using the formula:

$$Cell\ seeding\ efficiency\ (\%) = \frac{N_t - N_r}{N_t} \times 100\%$$

2.5.2. Cell viability assessment

After 1, 7, and 14 days of culture, the viability of the seeded BMSCs on ACM/GT scaffolds and GT scaffolds was evaluated using the Live & Dead Cell Viability Assay (Invitrogen, USA) following the manufacturer's instructions and examined by confocal microscopy (Nikon, Japan). In addition, DNA content was also used to further assess cell proliferation capacity by a total DNA quantification assay (PicoGreen dsDNA assay, Invitrogen, USA) following the manufacturer's protocols.

2.5.3. Cytotoxicity of scaffolds

To determine the cytotoxicity of ACM/GT scaffolds and GT scaffolds, BMSCs were seeded at a density of After 14 days of 2×10^4 cells/mL in the extract solutions (supernatant from ACM/GT scaffolds and GT scaffolds soaked in DMEM containing 10% fetal bovine serum for 72 h) and then culture for 7 days. Following the manufacturer's instructions, the cytotoxicity of scaffolds was measured using the cell counting kit-8 (CCK-8; Dojindo, Japan) and the value was presented by the average optical density (OD) of five wells with each experiment repeated three times.

2.5.4. Gene expression analyses

After 14 days of culture, the total RNA of each cell-scaffold construct (n = 5 per group) was isolated using TRIzol reagent (Life Technologies, USA) and the RNA concentration was measured using a NanoDrop system (Thermo Scientific, USA) based on the manufacture's protocol. Reverse transcription was performed with a cDNA synthesis kit and gene expression was analyzed quantitatively with the SYBR Green using LightCycler® 480 Real-Time PCR system (Roche Ltd) according to a previously established method [25]. Forward and reverse primer sequences for collagen type II alpha 1 (COL 2A1), aggrecan (ACAN), SRY-box transcription factor IX (SOX 9), and beta-actin housekeeping gene were designed based on published gene sequences from NCBI and PubMed (Table S1). Beta-actin was used as endogenous control and the expression levels for each gene were normalized with beta-actin and analyzed using the $2^{-\Delta\Delta CT}$ method as previously described.

2.6. Surgical procedures and grouping

2.6.1. Experimental grouping

Eighteen hybrid pigs were randomly divided into two groups in this study. In the first group, nine pigs were used to compare the effects of the ACM/GT scaffold group and untreated group in repairing full-thickness articular cartilage defects of 3 different sizes (4-, 6-, and 8-mm in diameter, Table S2). In the second group, nine pigs were used to compare the repair effects of the MNC-ACM/GT construct that immediately enriched mononuclear cells and the ACM/GT scaffold alone on full-thickness articular cartilage defects of different sizes (6-, 8-, and 10-mm in diameter, Table S3).

2.6.2. Isolation and enrichment of mononuclear cells

Bone marrow was aspirated from the anterior superior iliac spine of each animal under anesthetic and disinfection conditions. Mononuclear cells were isolated using density gradient centrifugation according to Ficoll-Paque's manufacturer's protocols [14]. Then, the mononuclear cell suspension was inoculated on the ACM/GT scaffold to form MNC-ACM/GT construct to instantly repair articular cartilage defects.

2.7. Repair of articular cartilage defects

As shown in Figure S1, hybrid pigs were anesthetized and two cylindrical full-thickness articular cartilage defects (4-, 6-, 8-, and 10-mm in diameter, chondral defects) were created using a trephine at the weight-bearing area of the femoral medial and lateral condyles of the knee joint as described previously [17]. After the removal of blood clots, both defects were repaired with the ACM/GT scaffold alone, with the MNC-ACM/GT construct, or left untreated according to the above grouping principles. Scaffolds and constructs were fixed in place by stitching to surrounding native cartilage with biodegradable sutures. All animals had only two defects in one knee joint, and the selection of medial or later condyles in different groups was random. All animals were allowed to move freely and regained normal gaits and locomotion after the operation. The animal care and use committee of Shanghai Jiaotong University School of Medicine approved all the animal studies for this research.

2.8. Gross observation and grading of the repaired regions

Six months after the operation, all pigs were euthanized to harvest repaired knee joints (distal part of femur). The harvested samples were first examined grossly and then sawed sagittal through the midline of the repaired regions to observe the interface healing between the repaired regions and the adjacent normal regions. Gross view results were graded into three scales: *complete repair, incomplete repair, and no repair* with criteria similar to those previously reported [26]. After gross observation, half of each specimen was used for histological examination, and the other half was used for quantification analysis.

2.9. Histological examination and grading of the repaired regions

The harvested samples were fixed, decalcified, embedded in paraffin, and sectioned into 5-mm slices for histological and immunohistochemical analyses according to our previously established methods [27]. The slices were stained with hematoxylin and eosin (H&E), safranin O and fast green (SO/FG), and type II collagen (COL II, polyclonal antibody ab34712, 1:100, Abcam, Cambridge, UK) to evaluate the histological structure and cartilage ECM deposition. The histological grading scores and International Cartilage Repair Society (ICRS) macroscopic evaluation of cartilage repair were also performed through blind analysis as previously reported methods (Table S4, S5) [28,29].

2.10. Biochemical, biomechanical, and RT–PCR analysis of the repaired tissues

Quantitative analysis of both regenerated tissues and native articular cartilage was performed as described previously [30]. The samples were collected and minced to conduct cartilage-related biochemical evaluations (n = 3). Briefly, glycosaminoglycan (GAG), hydroxyproline (HYP) content, and DNA quantifications were quantified by the dimethyl methylene blue assay (DMMB, Sigma–Aldrich), hydroxyproline assay kit (Sigma–Aldrich), and PicoGreen dsDNA assay (Invitrogen), respectively. Biomechanical analysis was performed by the above methods. The expression of chondrogenesis markers (COL 2A1, ACAN, and SOX 9) and hypertrophy-related markers (COL 1A1) was analyzed by RT–PCR, and relative expression levels were analyzed by the $2^{-\Delta\Delta CT}$ method as described above.

2.11. Statistical analysis

All quantitative data were collected from at least three replicate tests, and values are expressed as the mean ± standard deviation. After confirmation of normal data distribution, Student's t-test or one-way analysis of variance (ANOVA) was used to determine the statistical significance among groups using GraphPad Prism 8 software, and a value of $p < 0.05$ was considered statistically significant.

3. Results

3.1. Preparation and characterization of acellular cartilage matrix

The schematics in Fig. 1A showed the preparation process of ACM and ACM/GT scaffold. After a series of decellularization processes, ACM was successfully prepared and the effect of decellularization was further evaluated. The results of H&E staining showed that normal cellular structure with nucleus was observed in native cartilage tissue, but only the residual hollow lacuna-like structure was observed in the acellular sample (Fig. 1B). Meanwhile, DAPI staining also showed that the nucleus with blue fluorescence was presented in the native cartilage while disappeared in the acellular sample. Furthermore, as shown in Fig. 1C, DNA quantitative analysis further confirmed that more than 95% of DNA content was removed after the decellularization procedure. And the content of alpha-gal was decreased from 9.33 ± 0.25 U/mg to 0.65 ±

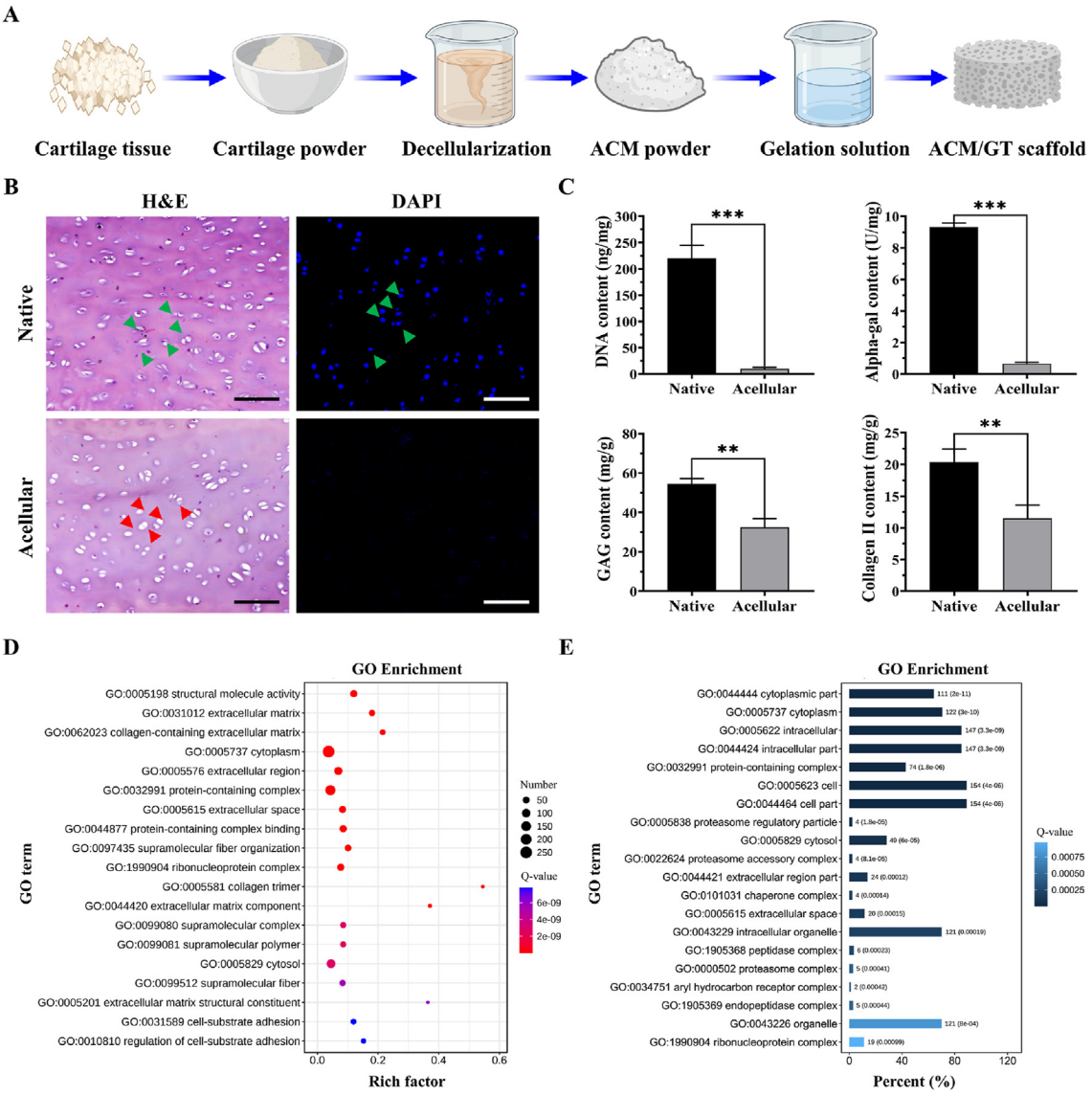

Fig. 1. Preparation and characterization of ACM. (A) The schematic of the preparation process of ACM and scaffolds. (B) H&E and DAPI staining of native cartilage and acellular cartilage (green arrows representing the cell nucleus and red arrows representing the remaining lacuna-like structures after decellularization). (C) Quantitative analysis of DNA content, alpha-gal content, GAG content, and collagen II content of native cartilage and acellular cartilage. GO enrichment analysis of the (D) preserved proteins and (E) lost proteins in ACM. Scale bar: 100 μm $^{**}p < 0.01$ and $^{***}p < 0.001$.

0.16 U/mg, which more than 90% of the alpha-gal content was removed. The removal of most of the DNA and alpha-gal content was conducive to minimizing the immune rejection after xenotransplantation in the future clinical translation. To confirm ECM preservation, the contents of GAG and collagen components in ACM were quantified, and the results showed that most of the GAG content (~59.53 ± 8.18%) and collagen II content (~56.43 ± 10.26%) were retained.

Furthermore, to identify the ECM components retained and lost after decellularization procedures, ACM and native cartilage were processed for proteomics analysis and revealed that 607 proteins were found in both native and ACM, while 458 unique proteins were found solely in native cartilage which was lost during decellularization procedures. To further determine the biological functions of these preserved and lost proteins, GO enrichment analysis was performed and the results showed that the preserved proteins in the ACM were mainly concentrated in ECM components, and played relevant biological functions such as *extracellular matrix*, *collagen-containing extracellular matrix*, *extracellular region*, *extracellular space*, *collagen trimer*, *extracellular matrix component*, etc. (Fig. 1D). Meanwhile, the lost proteins during decellularization procedures were mainly related to cellular components such as the *cytoplasmic part*, *intracellular part*, *cell part*, and *organelle part*, which further verified the effectiveness of decellularization (Fig. 1E). In summary, the proteomics results verified that most ECM-related components were preserved while cellular components were removed, and the functional enrichment analysis further provided strong evidence support for combination and modification to prepare more ideal biomimetic biomaterials and biological scaffolds for tissue engineering.

3.2. Characterization and biocompatibility of scaffolds

After analyzing the characterization, evaluating the suitability of scaffolds in tissue regeneration became the focus of the next step. As shown in Fig. 2A, both the ACM/GT scaffold and GT scaffold exhibited a spongy porous structure, and SEM examination also confirmed the porous surface. After inoculating BMSCs, the gross view showed that the porous structure of scaffolds could be filled and completely covered with cells (Fig. 2B). And SEM observation further confirmed that BMSCs were successfully seeded and adhered to the scaffolds (indicated by white

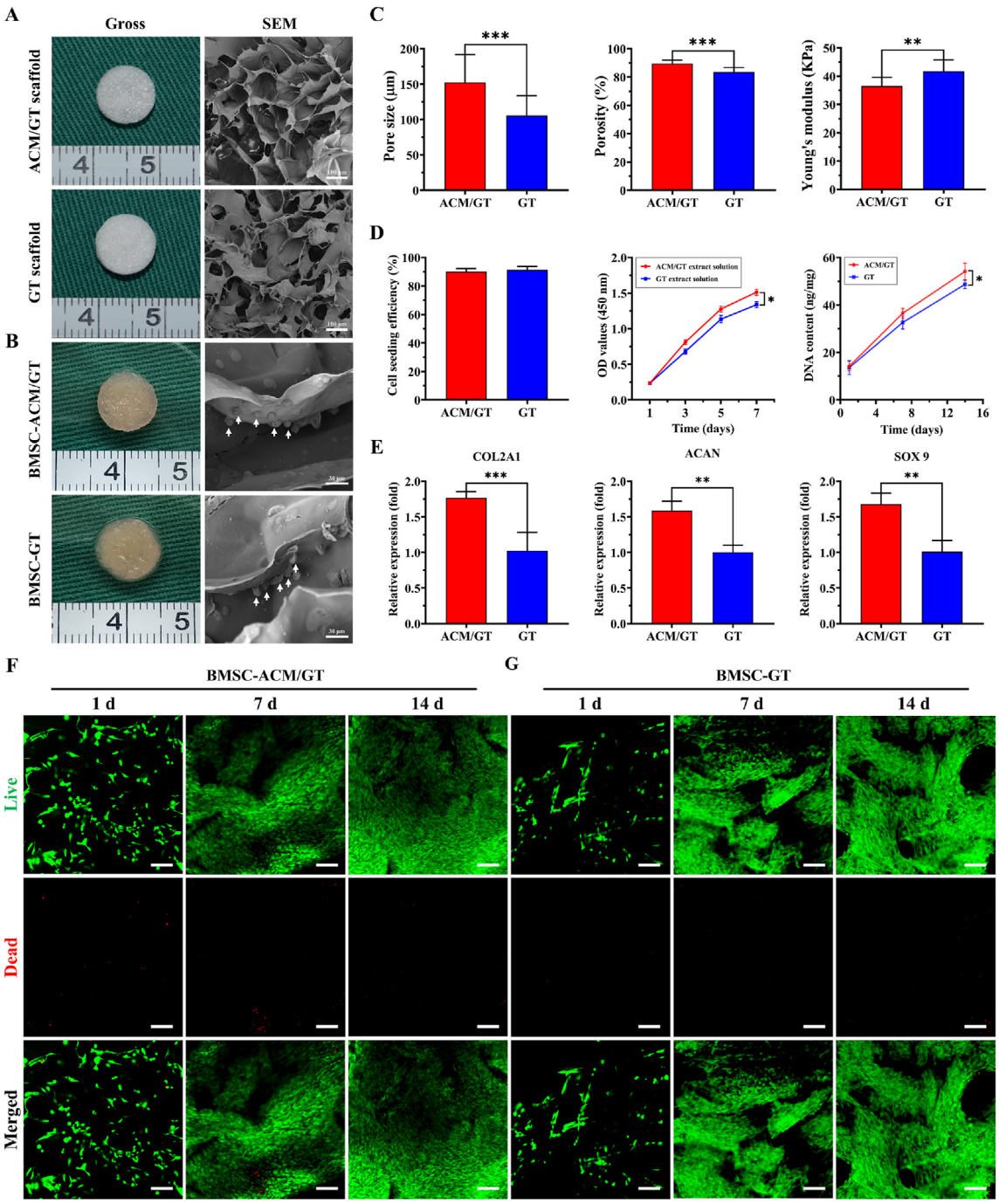

Fig. 2. Characterization and biocompatibility of scaffolds. Gross view and SEM images of (A) the ACM/GT scaffold and GT scaffold, as well as (B) BMSC-ACM/GT construct and BMSC-GT construct (the white arrows indicate the BMSCs adhered to the scaffolds). (C) Characterization analysis of pore size, porosity, and Young's modulus of the ACM/GT scaffolds and GT scaffolds. (D) Biocompatibility evaluation of cell seeding efficiency, cytotoxicity, and cell proliferation cell viability, as well as (E) the expression of chondrogenic genes (COL 2A1, ACAN, and SOX 9) of the BMSC-ACM/GT constructs and BMSC-GT constructs. Live & Dead staining showed that the number of cells on (F) BMSC-ACM/GT constructs and (G) BMSC-GT constructs gradually increased with the culture time. Green fluorescence and red fluorescence representing live cells and dead cells, respectively. Scale bar: 100 μm $^{*}p < 0.05$, $^{**}p < 0.01$, and $^{***}p < 0.001$.

arrows). As shown in Fig. 2C, characterization analysis further showed that the pore size and porosity of the ACM/GT scaffold were higher than those of the GT scaffold, but Young's modulus was slightly lower than that of the GT scaffold. In summary, both the ACM/GT scaffold and the GT scaffold meet the requirements of cartilage tissue regeneration. In contrast, the ACM/GT scaffold had a more suitable pore structure and may be more feasible for tissue regeneration by inoculating cells.

Cell seeding efficiency, cytotoxicity, cell proliferation, and the expression of chondrogenic genes were determined to evaluate the biocompatibility of scaffolds. As shown in Fig. 2D, the cell seeding efficiency of both the ACM/GT scaffold and the GT scaffold was more than 90%, and the cytotoxicity test further verified that the extract solution of the scaffold had no negative effect on cell survival and proliferation. Interestingly, the DNA content significantly increased with the culture time, and the ACM/GT group was significantly greater than the GT group, which suggested that the ACM had eligible biocompatibility for supporting cell proliferation. Notably, the relative expression of chondrogenic genes (COL 2A1, ACAN, and SOX 9) on the ACM/GT scaffold

was higher than that on the GT scaffold (Fig. 2E), indicating that ACM may have the potential to promote the differentiation of BMSCs into chondrocytes. Meanwhile, the Live/Dead staining showed that BMSCs grew well on both the ACM/GT scaffold and GT scaffold with the number of cells increasing significantly over time, and the cells had stretched and covered the entire scaffold surface by 14 days (Fig. 2F and G). Collectively, these results indicated that the ACM/GT scaffolds are more favorable for inoculating BMSCs to achieve differentiation into chondrocytes and regeneration into tissue-engineered cartilage.

3.3. Evaluation of ACM/GT scaffolds for repairing articular cartilage defects

3.3.1. Repair of articular cartilage defects with 4 mm in diameter

The schematics in Fig. 3A showed the surgical procedures to repair full-thickness articular cartilage defects with ACM/GT scaffolds and untreated control. Hybrid pigs with two cylindrical full-thickness articular cartilage defects (4-, 6-, and 8-mm in diameter, chondral defects) were used to compare the cartilage repair effects between the ACM/GT scaffold group and untreated group. For the cartilage repair effects with 4 mm in diameter, the defect in the ACM/GT (4) group was completely repaired with satisfactory cartilage-like tissue, and cross-sections showed that the defect was repaired with good interface healing to adjacent normal tissues (Fig. 3B). In contrast, the defect in the blank (4) group was slightly repaired with an irregular surface. Histological examinations of H&E, SO/FG, and COL II staining further confirmed these observations (Fig. 3C). The repaired regions in the ACM/GT (4) group exhibited relatively homogeneous hyaline cartilage-like histological features with mature cartilage lacuna and strong cartilage-specific ECM staining. However, the repaired regions in the blank (4) group mainly exhibited unrepaired tissue or fibrous-like histological features. In addition, the heatmap of gross view grading scores (Fig. 3D) and ICRS scores (Fig. 3E) provided the numerical distribution of reparative levels of the ACM/GT (4) group and blank (4) group. Three pigs in ACM/GT (4) group were *complete repair* by gross view grading, while none of the pigs was *complete repair* in the blank (4) group. Meanwhile, three pigs in ACM/GT (4) group achieved higher ICRS scores than the blank (4) group, indicating that the reparative effect of ACM/GT (4) was better than the blank (4) group.

3.3.2. Repair of articular cartilage defects with 6 mm in diameter

For the cartilage repair effects with 6 mm in diameter, the defect in the ACM/GT (6) group was mostly repaired with cartilage-like tissue and mixed with a small amount of fibrous-like tissue (Figure S2A). Cross-sections showed that the defect was mostly repaired with a relatively regular surface and interface healing to adjacent normal tissue. In contrast, the defect in the blank (6) group was mostly unrepaired with severely irregular surfaces. Histologically, the repaired regions in the ACM/GT (6) group mostly exhibited cartilage-like histological features

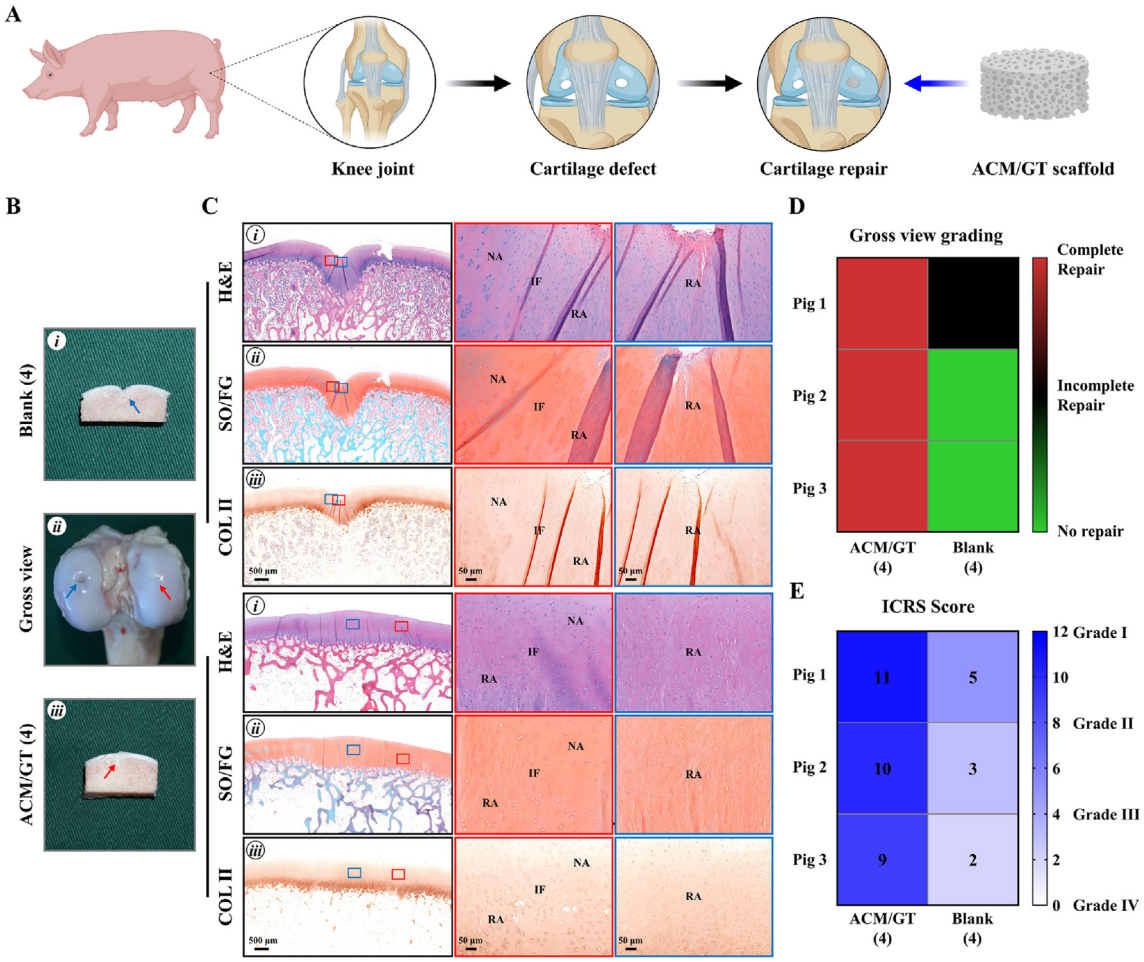

Fig. 3. Gross view and histological examination of the ACM/GT scaffolds for repairing articular cartilage defects with 4 mm in diameter. (A) The schematic of the surgical procedures to repair articular cartilage defects with ACM/GT scaffolds and untreated control. (B) Gross view and cross-sections of repaired articular cartilage defects after 6 months of the operation. Red arrows and blue arrows indicate the repaired regions of the ACM/GT (4) group and blank (4) group, respectively. (C) H&E, SO/FG, and COL II staining of repaired articular cartilage defects. Red rectangles and blue rectangles indicate the repaired areas and interface areas, respectively. RA: repaired area; IF: interface; NA: native area. (D) Gross view grading and (E) ICRS grading of the repair effect of ACM/GT (4) group and blank (4) group.

mixed with small fibrous-like histological features. Nevertheless, the repaired regions in the blank (6) group left obvious tissue defects or had a few fibrous-like histological features. Heatmap of gross view grading scores (Figure S2C) and ICRS scores (Figure S2D) provided the numerical distribution of reparative levels of the ACM/GT (6) group and blank (6) group. The results showed that two pigs in ACM/GT (6) group were *complete repair* and one pig was *incomplete repair* by gross view grading, while three pigs were all *no repair* in the blank (6) group. Meanwhile, three pigs in ACM/GT (6) group achieved higher ICRS scores than the blank (6) group, indicating that the reparative effect of ACM/GT (6) was better than the blank (6) group.

3.3.3. *Repair of articular cartilage defects with 8 mm in diameter*

As shown in Figure S3, the repaired region in the ACM/GT (8) group mainly consisted of disorganized fibrous-like tissue with a small amount of cartilage-like tissue. In contrast, the defects in the blank (8) group were mostly unrepaired and left obvious tissue defects. Histological examinations further supported the above observations that the repaired regions in the ACM/GT (8) group mostly exhibited fibrous-like histological features, and the repaired regions in the blank (8) group left obvious tissue defects, similar to the blank (6) group. Heatmap of gross view grading scores (Figure S3C) and ICRS scores (Figure S3D) showed that two pigs in ACM/GT (8) group were *incomplete repair* by gross view grading, while three pigs were all *no repair* in blank (8) group. Furthermore, three pigs in ACM/GT (8) group achieved higher ICRS scores than the blank (8) group, but neither of the two groups could achieve a satisfactory repair effect.

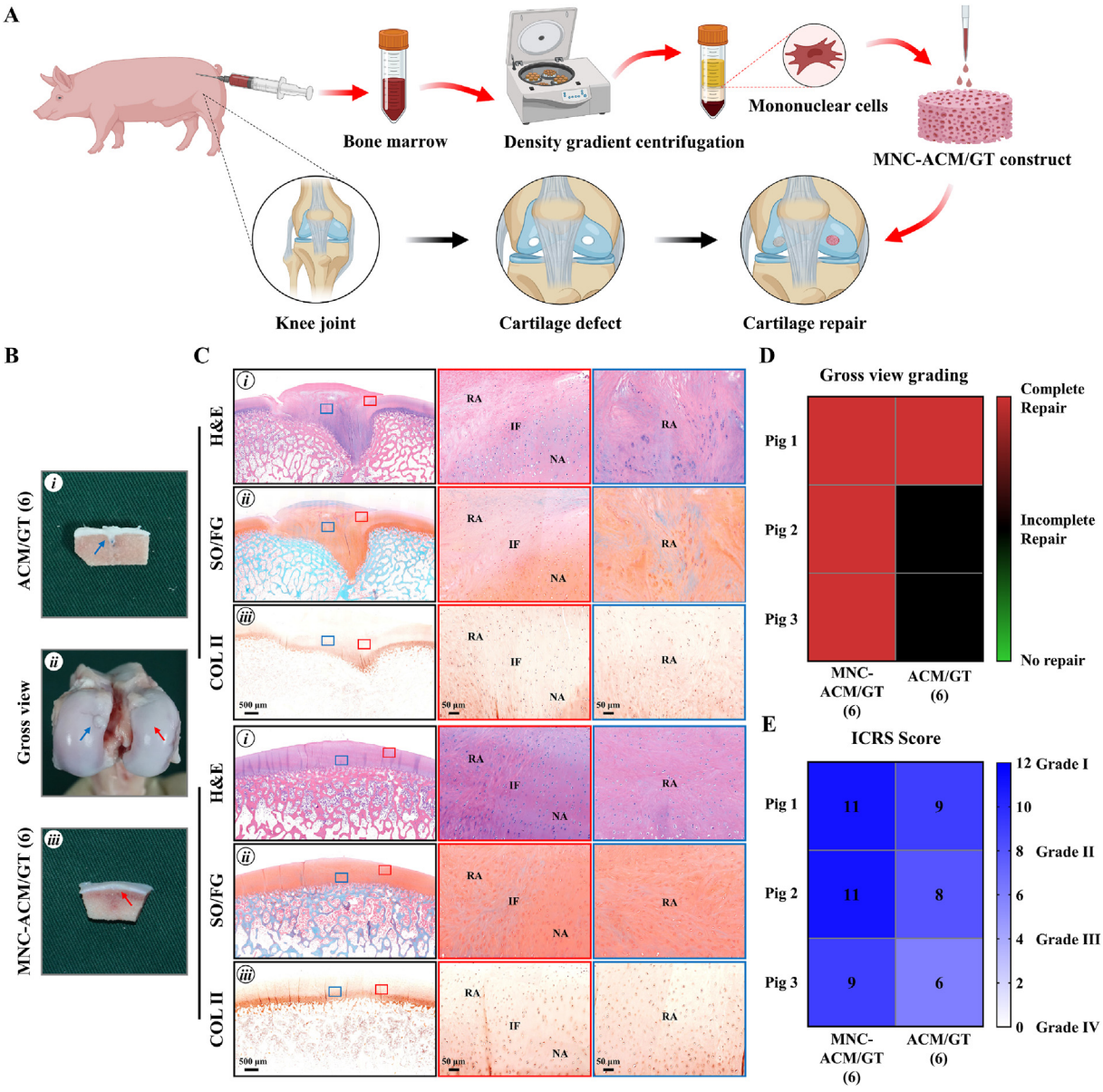

Fig. 4. Gross view and histological examination of MNC-ACM/GT constructs for repairing articular cartilage defects with 6 mm in diameter. (A) The schematic of the surgical procedures to repair articular cartilage defects with MNC-ACM/GT constructs and ACM/GT scaffolds. (B) Gross view and cross-sections of repaired articular cartilage defects after 6 months of the operation. Red arrows and blue arrows indicate the repaired regions of the MNC-ACM/GT (6) group and ACM/GT (6) group, respectively. (C) H&E, SO/FG, and COL II staining of repaired articular cartilage defects. Red rectangles and blue rectangles indicate the repaired areas and interface areas, respectively. RA: repaired area; IF: interface; NA: native area. (D) Gross view grading and (E) ICRS grading of the repair effect of the MNC-ACM/GT (6) group and ACM/GT (6) group.

3.4. Evaluation of the MNC-ACM/GT construct for repairing articular cartilage defects

3.4.1. Repair of articular cartilage defects with 6 mm in diameter

The schematics in Fig. 4A showed the surgical procedures to repair full-thickness articular cartilage defects using MNC-ACM/GT constructs which were immediately enriched with autologous BMMMCs and ACM/GT scaffolds. Hybrid pigs with two cylindrical full-thickness articular cartilage defects (6-, 8-, and 10-mm in diameter, chondral defects) were used to compare the cartilage repair effects between the MNC-ACM/GT construct group and ACM/GT scaffold group. Approximately 10 mL of fresh bone marrow was aspirated from the anterior superior iliac spine of each pig, and mononuclear cells were isolated using density gradient centrifugation according to the Ficoll-Paque's protocol. The proportion of mesenchymal stem cells is extremely low (approximately 0.0005% of all events in whole bone marrow) and density gradient centrifugation can significantly increase the ratio of MSCs by nearly a hundredfold. About 100,000 MSCs can be isolated from 10 mL of fresh bone marrow, and finally concentrated into about 100 μL of cell suspension and seeded on ACM/GT scaffolds for articular cartilage repair. And significantly improved results were observed in defects treated with MNC-ACM/GT constructs when compared to ACM/GT scaffolds. For the cartilage repair effects with 6 mm in diameter, the MNC-ACM/GT (6) group achieved the best results in that the defect was repaired completely with newly formed cartilage-like tissue and relatively smooth articular surfaces (Fig. 4B). Cross-sections showed that the new cartilage-like tissues were all well integrated into the surrounding cartilage with good interfacial healing. Histological examinations confirmed that the repaired regions exhibited relatively homogeneous hyaline cartilage-like histological features (Fig. 4C). In contrast, the defect in the ACM/GT (6) group was repaired with hybrid tissues comprising cartilage-like tissue and fibrous-like tissue, as described above. In addition, the heatmap of gross view grading scores (Fig. 4D) and ICRS scores (Fig. 4E) provided the numerical distribution of reparative levels of the MNC-ACM/GT (6) group and ACM/GT (6) group. Three pigs in MNC-ACM/GT (6) group were all *complete repair* by gross view grading. Meanwhile, three pigs in MNC-ACM/GT (6) group achieved higher ICRS scores than ACM/GT (6) group, indicating that the enrichment of MNCs could improve the repair effect of the ACM/GT scaffold.

3.4.2. Repair of articular cartilage defects with 8 mm in diameter

The MNC-ACM/GT (8) group achieved reparative results that were superior to those of the ACM/GT (8) group, and most of the defects in the MNC-ACM/GT (8) group were completely repaired by cartilage-like tissue (Fig. 5A). Cross-sections showed that the repaired tissues were well integrated into the surrounding cartilage with relatively good interfacial healing. Histological examinations mostly showed cartilage-like histological features with strong cartilage ECM staining (Fig. 5B). In addition, the uncontrollable removal of the calcified layer during defect creation might cause regenerated cartilage to embed into the subchondral bone. In contrast, the defects in the ACM/GT (8) group exhibited irregular surfaces with visible tissue deficits in some areas of the defects. Heatmap of gross view grading scores (Fig. 5C) and ICRS scores (Fig. 5D) provided the numerical distribution of reparative levels of the MNC-ACM/GT (8) group and ACM/GT (8) group. The results showed that two pigs were *complete repair* and one pig was *incomplete repair* in MNC-ACM/GT (6) group by gross view grading, while none of the pigs was *complete repair* in ACM/GT (8) group. Furthermore, three pigs in MNC-ACM/GT (8) group achieved higher ICRS scores than ACM/GT (8) group, indicating that the enrichment of MNCs could improve the repair effect of the ACM/GT

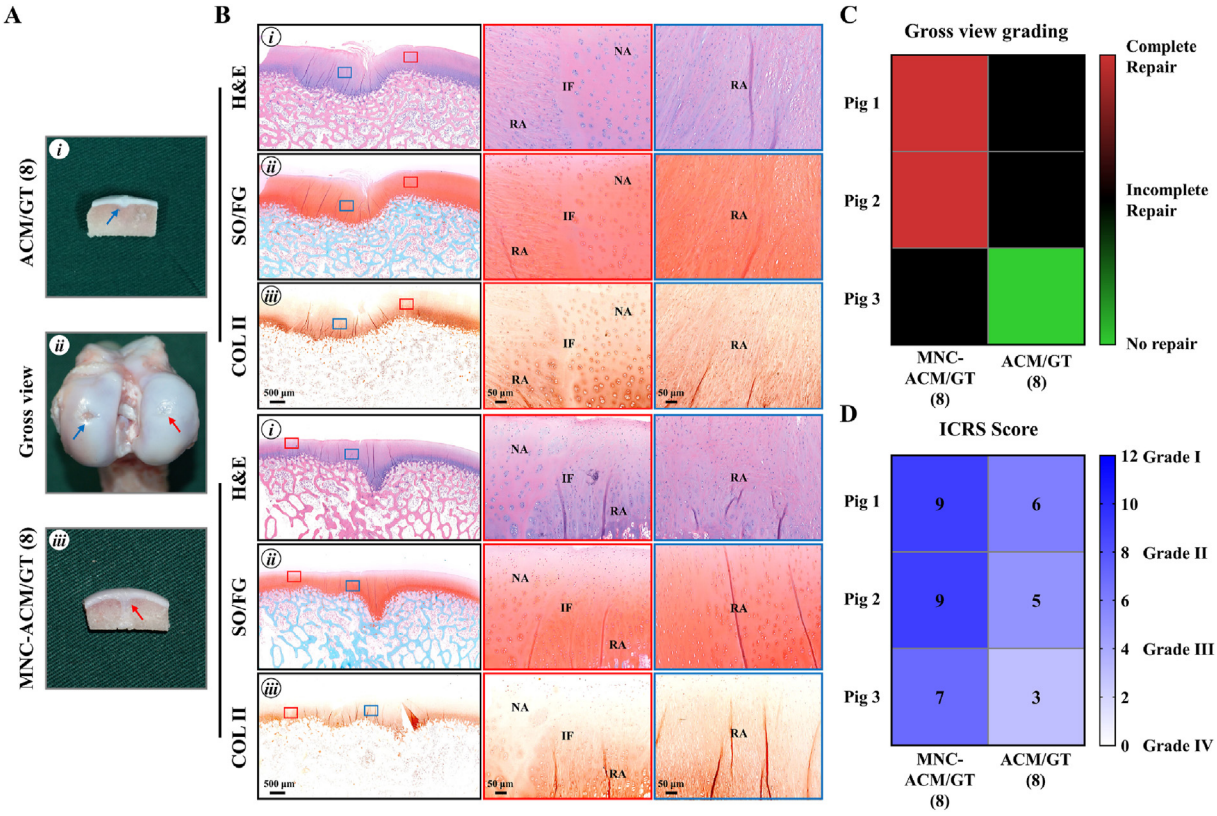

Fig. 5. Gross view and histological examination of MNC-ACM/GT constructs for repairing articular cartilage defects with 8 mm in diameter. (A) Gross view and cross-sections of repaired articular cartilage defects after 6 months of the operation. Red arrows and blue arrows indicate the repaired regions of the MNC-ACM/GT (8) group and ACM/GT (8) group, respectively. (B) H&E, SO/FG, and COL II staining of repaired articular cartilage defects. Red rectangles and blue rectangles indicate the repaired areas and interface areas, respectively. RA: repaired area; IF: interface; NA: native area. (C) Gross view grading and (D) ICRS grading of the repair effect of the MNC-ACM/GT (8) group and ACM/GT (8) group.

scaffold.

3.4.3. Repair of articular cartilage defects with 10 mm in diameter

For the cartilage repair effects with 10 mm, the repaired region in the MNC-ACM/GT (10) group mainly consisted of cartilage-like tissue with a small amount of fibrous-like tissue (Fig. 6A). Histological examinations further confirmed that the repaired region in the MNC-ACM/GT (10) group mostly exhibited cartilage-like histological features with positive staining of GAG and COL II (Fig. 6B). In contrast, the repaired region in the ACM/GT (10) group mainly consisted of fibrous tissue with obvious tissue disruption and an unsmooth surface. In addition, the defect was not completely repaired when observed at cross-sections, and the repaired region was mostly negative for GAG and COL II. Furthermore, the heatmap of gross view grading scores (Fig. 6C) and ICRS scores (Fig. 6D) provided the numerical distribution of reparative levels of the MNC-ACM/GT (10) group and ACM/GT (10) group. The results showed that two pigs were *incomplete repair* and one pig was *no repair* in MNC-ACM/GT (10) group by gross view grading, while one pig was *incomplete repair* and two pigs were *no repair* in ACM/GT (10) group. Three pigs in MNC-ACM/GT (10) group achieved higher histological grading scores than ACM/GT (10) group, indicating that the enrichment of MNCs could improve the repair effect, but neither of the two groups could achieve a satisfactory repair effect.

3.5. Histological grading and MRI tracking

As summarized, gross view grading scores (Table S6, S7), histological grading scores (Table S8, S9), and ICRS scores (Table S10, S11) provided the numerical distribution of reparative levels of different groups. As shown in Table S8, the ACM/GT group achieved lower histological grading scores than the blank group at the same defect size, indicating better reparative results than the blank group. Meanwhile, the scores increased gradually with increasing defect size in both the ACM/GT group and the blank group. The scores of the blank (6) and blank (8) were close to the maximum, implying that there was no repair in defect regions. Interestingly, the scores of the MNC-ACM/GT groups were much lower than those of the ACM/GT groups, and the scores increased with increasing defect size (Table S9). Likewise, the ICRS scores also showed that the repair effect of the ACM/GT group was significantly better than that of the blank group, and the repair effect of the MNC-ACM/GT group was better than that of the ACM/GT group (Table S10, S11). Importantly, the ACM/GT scaffold could repair articular cartilage defects 6 mm in diameter, while the MNC-ACM/GT construct could repair defects up to 8 mm in diameter. These phenomena indicate that the enrichment of MNCs could improve the repair effect of the ACM/GT scaffold alone and achieve a more satisfactory repair.

As shown in Figure S4, one of the same pigs in each part was tracked by MRI at different points in time (3 months and 6 months) to monitor the repaired regions. MRI revealed that the ACM/GT scaffold and MNC-ACM/GT construct in both groups were effectively retained in the repaired regions. Notably, articular cartilage regeneration in the ACM/GT scaffold group, especially in the MNC-ACM/GT construct group, presented a time-dependent trend, which was inferred from the evolution of the bright water signals (strong signals changed to weak signals), suggesting that the repair results improved gradually with post-repair time.

3.6. Quantitative analysis of the repaired tissues

The quantitative analysis of the repaired tissues further supports the

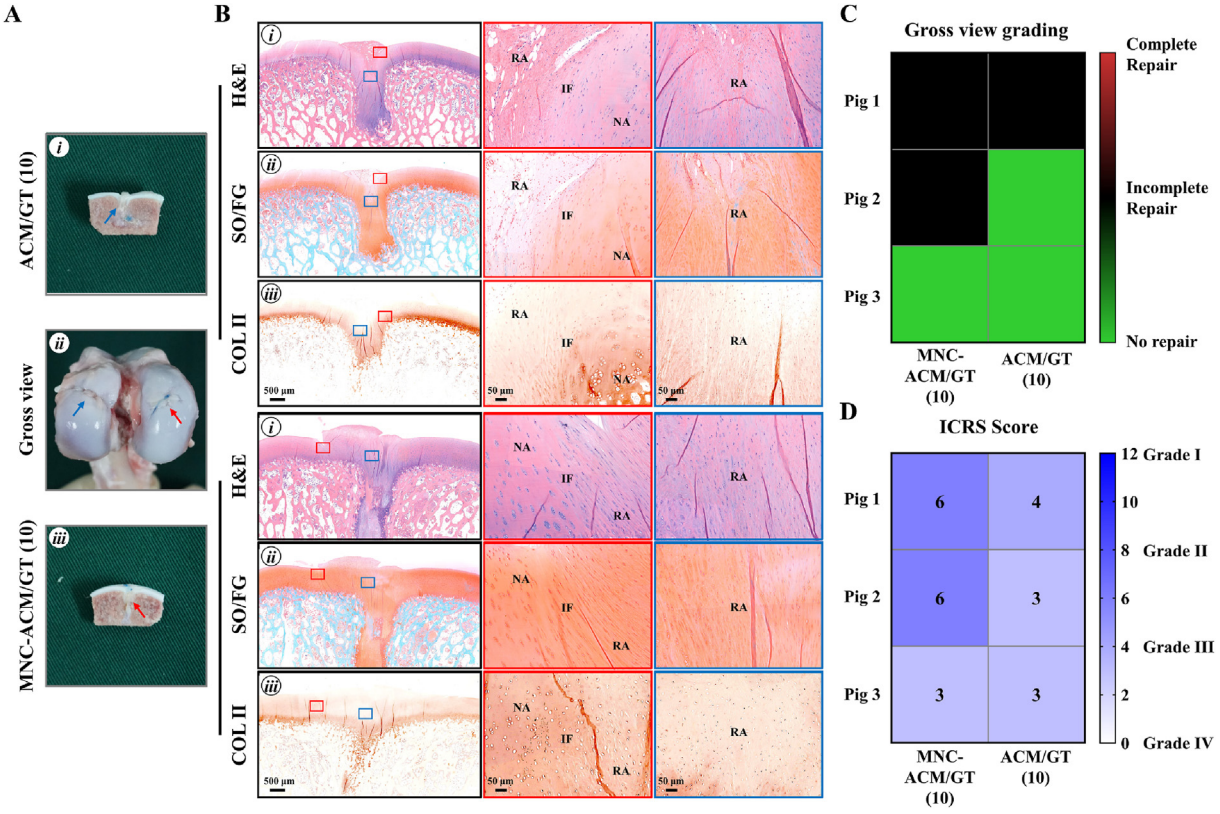

Fig. 6. Gross view and histological examination of MNC-ACM/GT constructs for repairing articular cartilage defects with 10 mm in diameter. (A) Gross view and cross-sections of repaired articular cartilage defects after 6 months of the operation. Red arrows and blue arrows indicate the repaired regions of the MNC-ACM/GT (10) group and ACM/GT (10) group, respectively. (B) H&E, SO/FG, and COL II staining of repaired articular cartilage defects. Red rectangles and blue rectangles indicate the repaired areas and interface areas, respectively. RA: repaired area; IF: interface; NA: native area. (C) Gross view grading and (D) ICRS grading of the repair effect of the MNC-ACM/GT (10) group and ACM/GT (10) group.

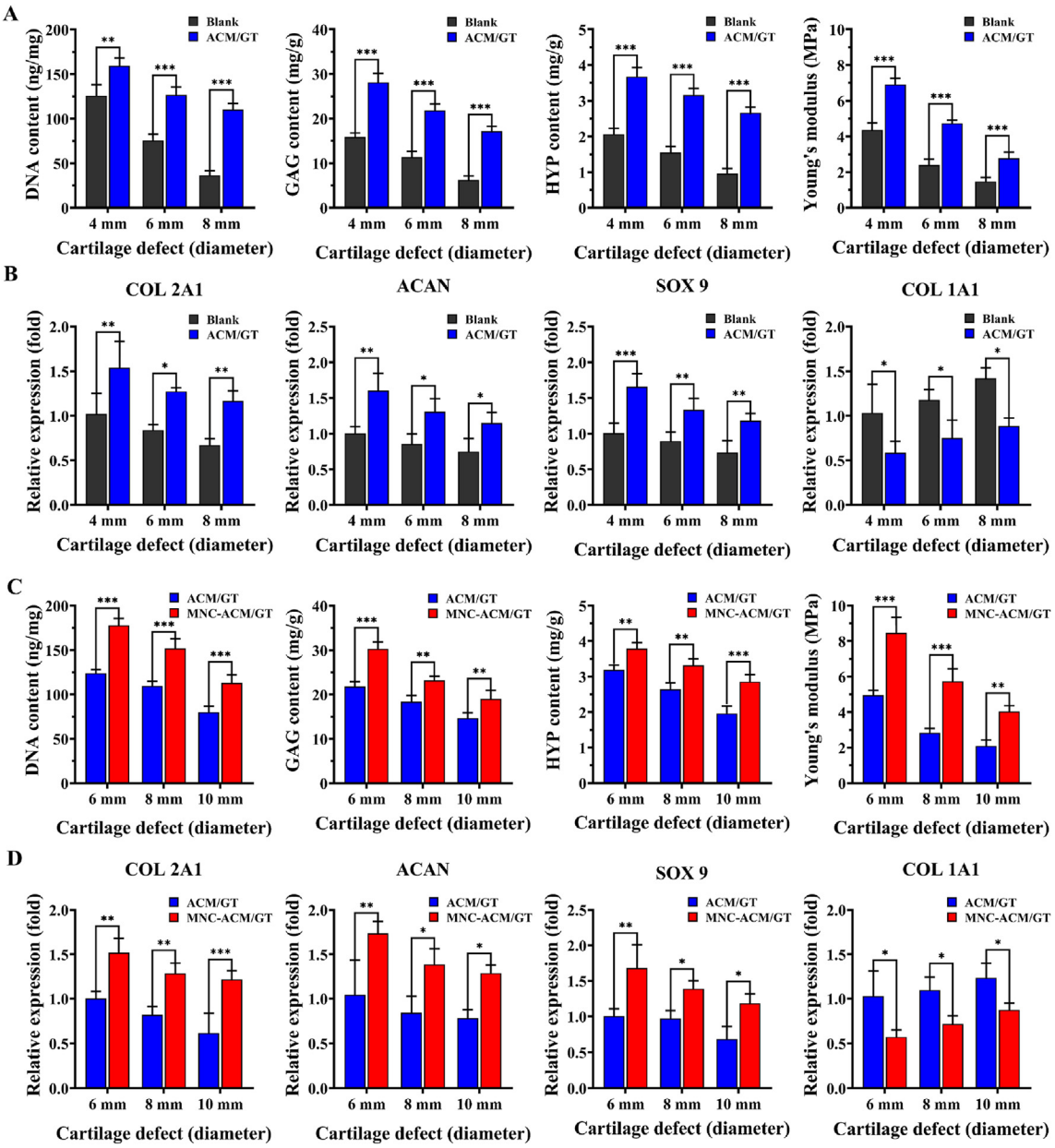

Fig. 7. Quantitative analysis of the repaired tissues. DNA content, GAG content, HYP content, Young's modulus, and the relative expression (fold change) of chondrogenic genes (COL 2A1, ACAN, and SOX 9) and hypertrophy-related gene (COL 1A1) in the ACM/GT & blank groups (A, B) and MNC-ACM/GT & ACM/GT groups (C, D), respectively. $*p < 0.05$, $**p < 0.01$, and $***p < 0.001$.

above results. As shown in Fig. 7A, the DNA content, GAG content, HYP content, and Young's modulus in the ACM/GT groups were significantly higher than those in the blank groups. In addition, the relative expression of chondrogenic genes (COL 2A1, ACAN, and SOX 9) in the ACM/GT groups was significantly higher than that in the blank groups, while the expression of the hypertrophy-related gene (COL 1A1) in the ACM/GT groups was significantly lower than that in the blank groups (Fig. 7B), indicating that the ACM/GT scaffold might not only promote chondrogenic differentiation but also inhibit endochondral ossification potential. Most importantly, the DNA content, GAG content, HYP content, and Young's modulus in the MNC-ACM/GT groups were significantly higher than those in the ACM/GT groups (Fig. 7C). Similarly, the expression levels of cartilage-specific genes (COL 2A1, ACAN, and SOX 9) rapidly increased and achieved a higher level in the MNC-ACM/GT groups than in the ACM/GT groups (Fig. 7D). Surprisingly, the hypertrophy-related gene (COL 1A1) significantly decreased in the MNC-ACM/GT groups. These results indicated that the enrichment of MNCs might directly participate in articular cartilage regeneration and improve the efficacy of articular defect repair.

4. Discussion

Articular cartilage damage and degeneration caused by injury, disease, and population aging are very common clinically, and there is a great clinical need for the regeneration and repair of articular cartilage [31–33]. Despite the great achievements of tissue engineering technology for cartilage repair [34–37], it has not become the mainstream technology of articular cartilage repair thus far. This is mainly due to the key bottlenecks of limited cell sources and scaffold materials. Autologous chondrocytes are difficult to popularize in the clinic because of the limited donor source and large trauma. Therefore, the source of cells with minimal trauma and immediate application is the first choice for clinical

application.

Since the first isolation and identification in the 1960s, MSCs have been recognized as the predominant component in the microenvironment, and have proverbially attracted the attention in both fundamental research and clinical applications, which is of great significance to the development of regenerative medicine [38]. Among them, bone marrow-derived mesenchymal stem cells are one of the most recognized sources of mesenchymal stem cells with multiple applications and long-term proliferation properties. However, autologous bone marrow stromal cells need additional isolation and culture processes [39,40], which cannot achieve immediate repair of cartilage defects such as acute trauma. In this research, the aspirated bone marrow was processed by density gradient centrifugation to obtain MNCs [41,42], a heterogeneous cell population that can be directly enriched into scaffolds for in vivo experiments. In addition, the final bone marrow concentration preparation has an increased concentration of progenitor/stem cells, growth factors, and cytokines, which may potentially have anabolic and anti-inflammatory effects on the damaged articular cartilage.

In addition, a proper biological scaffold with good biocompatibility is even more essential in cartilage regeneration. Hence, there is a tremendous need to develop ideal biomaterials that are capable of serving as powerful artificial niches to recruit, program, and direct host cells *in situ* for tissue regeneration purposes. Therefore, biomimetic scaffolds that can accurately mimic the native cartilage ECM will contribute to the regeneration of high-quality cartilage tissue. ACM, which is considered to be the ideal scaffold with a cartilage-specific microenvironment [43–45], was fabricated into a three-dimensional porous scaffold to determine the feasibility of repairing articular cartilage defects and the maximum scope of application. ACM scaffolds could provide a viable microenvironment for MSC attachment, proliferation, and differentiation into chondrocytes. Various stem cells are integrated into scaffolds to promote cartilage regeneration, which is a classic cartilage regeneration therapeutic strategy. The formation of cartilage may be due to spontaneous cell migration in the joint environment, and we speculate that this fraction of endogenous cells is derived from the stem or progenitor cells from the bone marrow, the synovium, the adipose (fat pad adjacent to the synovium and bone marrow), and perhaps vasculature, which have the better chondrogenic potential [2]. In the case of cartilage repair, stem/progenitor cells may initiate targeted repair systems that promote trophic effects by releasing synthetic, proliferative, and regenerative factors directly into cartilage damage, and create a regenerative environment by releasing chemokines [46]. The evaluation of repairing articular cartilage defects in hybrid pig models confirmed that the ACM-based scaffold can repair articular cartilage defects within 6 mm in diameter, but the effect is not satisfactory for a larger range of articular cartilage defects. This may be due to the lack of endogenous stem cells caused by the large range of defects, which cannot meet the requirement of repairing the cartilage defects completely.

To solve this problem of limited endogenous stem cells, the concentration of MNCs in bone marrow was increased nearly a hundredfold by density gradient centrifugation. Autologous MNCs were supplemented externally to significantly increase the initial number of stem cells in the biomimetic scaffold, which provides a sufficient source of stem cells for articular cartilage regeneration *in situ*. Most importantly, the operation of cell enrichment is fast and does not affect immediate application and repair at all. The biomimetic scaffold enriched in mononuclear cells by density gradient centrifugation can repair articular cartilage defects within 8 mm in diameter, which significantly improves the effect of articular cartilage repair *in situ*, indicating that the enrichment of mononuclear cells is important for satisfactory articular cartilage repair.

MNCs carried out various functions in the treatment of cartilage damage which include of increase of chondrogenesis, the proliferation of chondrocyte, reduction of apoptosis, maintenance of autophagy, regulation of synthesis and catabolism of the ECM, regulation of immune response, inhibition of inflammation, monitoring the mitochondrial dysfunction, and the paracrine effect. These functions were partly demonstrated through several biological pathways or axis, such as NF-κB, MAPK, ROS, and mTOR pathways [47]. Besides having excellent properties for regeneration, immunomodulatory properties are also one superior characteristic. This makes MNCs a promising cell source to repair cartilage defects and at the same time provide an immunomodulatory effect to reduce inflammation. Since the implanted cells are derived from the patient's autologous fresh bone marrow, they can survive for a long time after implantation and integrate well with the surrounding native tissues, so it is expected to achieve articular cartilage regeneration and permanent functional reconstruction.

Therefore, proposing a step-by-step multimodal tissue regeneration and clinical repair strategy according to the severity of articular cartilage defects: 1) For small-scale localized articular cartilage defects, where there are sufficient endogenous stem cells in the defect area, the ACM-based biomimetic scaffold could be used to induce tissue regeneration *in situ* and achieve articular cartilage repair; 2) For a large range of localized defects, where the local endogenous stem cells are relatively insufficient, through instant MNC enrichment technology, exogenously supplemented with autologous stem cells to significantly increase the initial number of stem cells in the ACM-based biomimetic scaffold, and then implanted into the defect site to induce tissue regeneration *in situ* and achieve articular cartilage repair; 3) For a larger range of defects where the local endogenous stem cell are severely deficient, in the next study, slow-release microspheres with active factors will be loaded to construct a multifunctional cartilage regeneration microenvironment, such as stromal cell-derived factor-1 (SDF-1) [48,49], transforming growth factor beta (TGF-β) [50,51], and insulin-like growth factor-1 (IGF-1) [52,53], to further recruit endogenous stem cells into the biomimetic scaffold, induce cartilage differentiation and cartilage formation, and maintain the stability of regenerated cartilage.

Despite the potential application of MNCs, much remains to be investigated such as the number of cells required to promote cartilage regeneration, the optimal time window for these treatments, and the long-term safety of the technique [54]. Meanwhile, it remains to be seen how these techniques compare with more established procedures in comparative clinical studies. It's worth noting that different loading conditions and mechanical environments result in cartilage regeneration and anatomical characteristic discrepancies. The articular surface is divided into weight-bearing and non-weight-bearing areas according to the force distribution of the joint surface. In knee joints, the medial and lateral condyles belong to the weight-bearing area, while the intercondylar and supracondylar fossa belongs to the non-weight-bearing area. The cartilage could be better repaired in weight-bearing conditions than in non-weight-bearing ones, which can be explained by the loading force transporting biological signals and activating the proliferation and differentiation abilities. And in the same joint, the external environment of the lateral and medial condyles is not much different [55]. Therefore, in this study, only one joint (including the medial condyle and the later condyle) per pig is used for experiments. It is worth noting that the final result shows the consistent difference between the experimental group and the control group, not the difference between the medial condyle and the later condyle, which is sufficient to demonstrate that the choice of location has little effect on the repair of cartilage defects.

In addition to mechanical effects, structural biomimicry is considered a critical factor in the selection of biomaterials for cartilage tissue repair to obtain properties similar to native cartilage. Heterogeneous and anisotropic articular cartilage is generally studied as a hierarchical structure of zones with unique composition and architecture. Articular cartilage consists of superficial, transitional, radial, and calcified cartilage zones [56]. The cellular phenotype and cartilage matrix distribution also changed in different layers. The rapid development of bioprinting technology has brought new possibilities for cartilage regeneration, which allows the fabrication of bioactive scaffolds with micrometer-scaled accuracy. By controlling the composition and arrangement of seed cells and carriers to design and produce specific

bioactive scaffolds with different structures, full-thickness cartilage that mimics the natural structure of cartilage tissue can be constructed. In a previous study, the cartilage acellular matrix has been successfully prepared into a bioink suitable for bioprinting [57]. In the following studies, according to the natural fiber distribution in natural cartilage, the geometric modules and unit compactness will be precisely pre-designed to simulate the cartilage micromorphology as perfectly as possible, and finally, the biomimetic structure and mechanical cartilage tissue scaffold will be constructed.

In conclusion, this study established repair models of articular cartilage defects of different sizes to determine the feasibility and maximum application range of ACM-based biomimetic scaffolds to induce regeneration of articular cartilage *in situ*. Furthermore, immediate enrichment of MNCs to repair articular cartilage defects clarified the feasibility of improving the repair effect of articular cartilage defects, which established a new model of articular cartilage regeneration that could be applied immediately and suited for large-scale clinical promotion, as well as overcoming the disadvantages of the existing treatment methods. It significantly improves the effect of defect repair and brings good news for tens of millions of patients with articular cartilage damage, which is of great scientific value and clinical significance.

5. Conclusions

In summary, the current study determined the feasibility and maximum scope of application of ACM-based biomimetic scaffolds to induce articular cartilage regeneration *in situ* through repair models of articular cartilage defects of different sizes in hybrid pigs. Furthermore, immediate enrichment of MNCs by the density gradient centrifugation method clarified the improvement of the repair effect in articular cartilage defects, establishing a new model of articular cartilage regeneration and functional reconstruction, which overcomes the disadvantages of the existing treatment methods and can be applied immediately. Although the effect of repair is still insufficient in larger defects, the current results have brought good news for tens of millions of patients with articular cartilage damage, which is of great scientific value and clinical significance.

Credit author statement

Litao Jia: Conceptualization, Methodology, Data curation, Visualization, Investigation, Writing – original draft. Peiling Zhang: Conceptualization, Methodology, Data curation, Investigation. Zheng Ci: Conceptualization, Methodology, Data curation, Investigation. Xiaoyan Hao: Methodology, Visualization. Baoshuai Bai: Methodology, Software, Data curation. Wei Zhang: Methodology, Visualization. Haiyue Jiang: Conceptualization, Methodology, Funding acquisition, Supervision, Writing – review & editing. Guangdong Zhou: Conceptualization, Methodology, Funding acquisition, Supervision, Writing – review & editing.

Declaration of competing interest

The authors declare that they have no known competing financial interests or personal relationships that could have appeared to influence the work reported in this paper.

Acknowledgments

This work was supported by the National Key Research and Development Program of China (2017YFC1103900, 2018YFC1005800), the National Natural Science Foundation of China (81871502), and the Chinese Academy of Medical Sciences Innovation Fund for Medical Sciences (2017-I2M-1-007, 2021-I2M-1-052).

Appendix A. Supplementary data

Supplementary data to this article can be found online at https://doi.org/10.1016/j.mtbio.2022.100310.

References

[1] D.J. Huey, J.C. Hu, K.A. Athanasiou, Unlike bone, cartilage regeneration remains elusive, Science 338 (6109) (2012) 917–921, https://doi.org/10.1126/science.1222454.
[2] C.H. Lee, J.L. Cook, A. Mendelson, E.K. Moioli, H. Yao, J.J. Mao. Regeneration of the articular surface of the rabbit synovial joint by cell homing: a proof of concept study, Lancet 376 (9739) (2010) 440–448, https://doi.org/10.1016/S0140-6736(10)60668-X.
[3] A.R. Merriam, J.M. Patel, B.M. Culp, C.J. Gatt Jr., M.G. Dunn, Successful total meniscus reconstruction using a novel fiber-reinforced scaffold: a 16- and 32-week study in an ovine model, Am. J. Sports Med. 43 (10) (2015) 2528–2537, https://doi.org/10.1177/0363546515595065.
[4] M. Brittberg, Autologous chondrocyte implantation–technique and long-term follow-up, Injury 39 (Suppl 1) (2008) S40–S49, https://doi.org/10.1016/j.injury.2008.01.040.
[5] J. Klein, Chemistry. Repair or replacement–a joint perspective, Science 323 (5910) (2009) 47–48, https://doi.org/10.1126/science.1166753.
[6] C. Feng, X. Luo, N. He, H. Xia, X. Lv, X. Zhang, D. Li, F. Wang, J. He, L. Zhang, X. Lin, L. Lin, H. Yin, J. He, J. Wang, W. Cao, R. Wang, G. Zhou, W. Wang, Efficacy and persistence of allogeneic adipose-derived mesenchymal stem cells combined with hyaluronic acid in osteoarthritis after intra-articular injection in a sheep model, Tissue Eng. 24 (3–4) (2018) 219–233, https://doi.org/10.1089/ten.TEA.2017.0039.
[7] E.A. Makris, A.H. Gomoll, K.N. Malizos, J.C. Hu, K.A. Athanasiou, Repair and tissue engineering techniques for articular cartilage, Nat. Rev. Rheumatol. 11 (1) (2015) 21–34, https://doi.org/10.1038/nrrheum.2014.157.
[8] S. Marlovits, P. Zeller, P. Singer, C. Resinger, V. Vecsei, Cartilage repair: generations of autologous chondrocyte transplantation, Eur. J. Radiol. 57 (1) (2006) 24–31, https://doi.org/10.1016/j.ejrad.2005.08.009.
[9] C. Ding, Z. Qiao, W. Jiang, H. Li, J. Wei, G. Zhou, K. Dai, Regeneration of a goat femoral head using a tissue-specific, biphasic scaffold fabricated with CAD/CAM technology, Biomaterials 34 (28) (2013) 6706–6716, https://doi.org/10.1016/j.biomaterials.2013.05.038.
[10] P. Occhetta, S. Pigeot, M. Rasponi, B. Dasen, A. Mehrkens, T. Ullrich, I. Kramer, S. Guth-Gundel, A. Barbero, I. Martin, Developmentally inspired programming of adult human mesenchymal stromal cells toward stable chondrogenesis, Proc. Natl. Acad. Sci. U. S. A. 115 (18) (2018) 4625–4630, https://doi.org/10.1073/pnas.1720658115.
[11] A.M. Craft, J.S. Rockel, Y. Nartiss, R.A. Kandel, B.A. Alman, G.M. Keller, Generation of articular chondrocytes from human pluripotent stem cells, Nat. Biotechnol. 33 (6) (2015) 638–645, https://doi.org/10.1038/nbt.3210.
[12] A. He, L. Liu, X. Luo, Y. Liu, Y. Liu, F. Liu, X. Wang, Z. Zhang, W. Zhang, W. Liu, Y. Cao, G. Zhou, Repair of osteochondral defects with in vitro engineered cartilage based on autologous bone marrow stromal cells in a swine model, Sci. Rep. 7 (2017) 40489, https://doi.org/10.1038/srep40489.
[13] D. Li, L. Zhu, Y. Liu, Z. Yin, Y. Liu, F. Liu, A. He, S. Feng, Y. Zhang, Z. Zhang, W. Zhang, W. Liu, Y. Cao, G. Zhou, Stable subcutaneous cartilage regeneration of bone marrow stromal cells directed by chondrocyte sheet, Acta Biomater. 54 (2017) 321–332, https://doi.org/10.1016/j.actbio.2017.03.031.
[14] F. Du, H. Wu, H. Li, L. Cai, Q. Wang, X. Liu, R. Xiao, N. Yin, Y. Cao, Bone marrow mononuclear cells combined with beta-tricalcium phosphate granules for alveolar cleft repair: a 12-month clinical study, Sci. Rep. 7 (1) (2017) 13773, https://doi.org/10.1038/s41598-017-12602-1.
[15] B.R. Freedman, D.J. Mooney, Biomaterials to mimic and heal connective tissues, Adv. Mater. 31 (19) (2019), e1806695, https://doi.org/10.1002/adma.201806695.
[16] Y. Li, Y. Xiao, C. Liu, The horizon of materiobiology: a perspective on material-guided cell behaviors and tissue engineering, Chem. Rev. 117 (5) (2017) 4376–4421, https://doi.org/10.1021/acs.chemrev.6b00654.
[17] J. Xue, A. He, Y. Zhu, Y. Liu, D. Li, Z. Yin, W. Zhang, W. Liu, Y. Cao, G. Zhou, Repair of articular cartilage defects with acellular cartilage sheets in a swine model, Biomed. Mater. 13 (2) (2018), 025016, https://doi.org/10.1088/1748-605X/aa99a4.
[18] L. Jia, Y. Zhang, L. Yao, P. Zhang, Z. Ci, W. Zhang, C. Miao, X. Liang, A. He, Y. Liu, S. Tang, R. Zhang, X. Wang, Y. Cao, G. Zhou, Regeneration of human-ear-shaped cartilage with acellular cartilage matrix-based biomimetic scaffolds, Appl. Mater. Today 20 (2020) 100639, https://doi.org/10.1016/j.apmt.2020.100639.
[19] Y.Y. Gong, J.X. Xue, W.J. Zhang, G.D. Zhou, W. Liu, Y. Cao, A sandwich model for engineering cartilage with acellular cartilage sheets and chondrocytes, Biomaterials 32 (9) (2011) 2265–2273, https://doi.org/10.1016/j.biomaterials.2010.11.078.
[20] J.X. Xue, Y.Y. Gong, G.D. Zhou, W. Liu, Y. Cao, W.J. Zhang, Chondrogenic differentiation of bone marrow-derived mesenchymal stem cells induced by acellular cartilage sheets, Biomaterials 33 (24) (2012) 5832–5840, https://doi.org/10.1016/j.biomaterials.2012.04.054.
[21] L. Jia, P. Zhang, Z. Ci, W. Zhang, Y. Liu, H. Jiang, G. Zhou, Immune-inflammatory responses of an acellular cartilage matrix biomimetic scaffold in a xenotransplantation goat model for cartilage tissue engineering, Front. Bioeng. Biotechnol. 9 (2021) 667161, https://doi.org/10.3389/fbioe.2021.667161.

[22] Y. Xu, Y. Guo, Y. Li, Y. Huo, Y. She, H. Li, Z. Jia, G. Jiang, G. Zhou, Z. You, L. Duan, Biomimetic trachea regeneration using a modular ring strategy based on poly(sebacoyl Diglyceride)/polycaprolactone for segmental trachea defect repair, Adv. Funct. Mater. 30 (42) (2020) 2004276, https://doi.org/10.1002/adfm.202004276.
[23] Y. Xu, L. Duan, Y. Li, Y. She, J. Zhu, G. Zhou, G. Jiang, Y. Yang, Nanofibrillar decellularized wharton's jelly matrix for segmental tracheal repair, Adv. Funct. Mater. 30 (14) (2020) 1910067, https://doi.org/10.1002/adfm.201910067.
[24] M. Hou, B. Tian, B. Bai, Z. Ci, Y. Liu, Y. Zhang, G. Zhou, Y. Cao, Dominant role of in situ native cartilage niche for determining the cartilage type regenerated by BMSCs, Bioact. Mater. (2021), https://doi.org/10.1016/j.bioactmat.2021.11.007.
[25] J. Hao, B. Bai, Z. Ci, J. Tang, G. Hu, C. Dai, M. Yu, M. Li, W. Zhang, Y. Zhang, W. Ren, Y. Hua, G. Zhou, Large-sized bone defect repair by combining a decalcified bone matrix framework and bone regeneration units based on photo-crosslinkable osteogenic microgels, Bioact. Mater. (2021), https://doi.org/10.1016/j.bioactmat.2021.12.013.
[26] G. Zhou, W. Liu, L. Cui, X. Wang, T. Liu, Y. Cao, Repair of porcine articular osteochondral defects in non-weightbearing areas with autologous bone marrow stromal cells, Tissue Eng. 12 (11) (2006) 3209–3221, https://doi.org/10.1089/ten.2006.12.3209.
[27] Y. Hua, H. Xia, L. Jia, J. Zhao, D. Zhao, X. Yan, Y. Zhang, S. Tang, G. Zhou, L. Zhu, Q. Lin, Ultrafast, tough, and adhesive hydrogel based on hybrid photocrosslinking for articular cartilage repair in water-filled arthroscopy, Sci. Adv. 7 (35) (2021), eabg0628, https://doi.org/10.1126/sciadv.abg0628.
[28] S. Wakitani, T. Goto, S.J. Pineda, R.G. Young, J.M. Mansour, A.I. Caplan, V.M. Goldberg, Mesenchymal cell-based repair of large, full-thickness defects of articular cartilage, J. Bone Joint Surg. Am. 76 (4) (1994) 579–592, https://doi.org/10.2106/00004623-199404000-00013.
[29] S. Pineda, A. Pollack, S. Stevenson, V. Goldberg, A. Caplan, A semiquantitative scale for histologic grading of articular cartilage repair, Acta Anat. 143 (4) (1992) 335–340, https://doi.org/10.1159/000147272.
[30] Y. Xu, Y. Xu, B. Bi, M. Hou, L. Yao, Q. Du, A. He, Y. Liu, C. Miao, X. Liang, X. Jiang, G. Zhou, Y. Cao, A moldable thermosensitive hydroxypropyl chitin hydrogel for 3D cartilage regeneration in vitro and in vivo, Acta Biomater. 108 (2020) 87–96, https://doi.org/10.1016/j.actbio.2020.03.039.
[31] A.A. Nurul, M. Azlan, M.R. Ahmad Mohd Zain, A.A. Sebastian, Y.Z. Fan, M.B. Fauzi, Mesenchymal stem cells: current concepts in the management of inflammation in osteoarthritis, Biomedicines 9 (7) (2021), https://doi.org/10.3390/biomedicines9070785.
[32] R. Xie, H. Yao, A.S. Mao, Y. Zhu, D. Qi, Y. Jia, M. Gao, Y. Chen, L. Wang, D.A. Wang, K. Wang, S. Liu, L. Ren, C. Mao, Biomimetic cartilage-lubricating polymers regenerate cartilage in rats with early osteoarthritis, Nat. Biomed. Eng. 5 (10) (2021) 1189–1201, https://doi.org/10.1038/s41551-021-00785-y.
[33] S. Jiang, G. Tian, Z. Yang, X. Gao, F. Wang, J. Li, Z. Tian, B. Huang, F. Wei, X. Sang, L. Shao, J. Zhou, Z. Wang, S. Liu, X. Sui, Q. Guo, W. Guo, X. Li, Enhancement of acellular cartilage matrix scaffold by Wharton's jelly mesenchymal stem cell-derived exosomes to promote osteochondral regeneration, Bioact. Mater. 6 (9) (2021) 2711–2728, https://doi.org/10.1016/j.bioactmat.2021.01.031.
[34] W. Chen, S. Chen, Y. Morsi, H. El-Hamshary, M. El-Newhy, C. Fan, X. Mo, Superabsorbent 3D scaffold based on electrospun nanofibers for cartilage tissue engineering, ACS Appl. Mater. Interfaces 8 (37) (2016) 24415–24425, https://doi.org/10.1021/acsami.6b06825.
[35] S. Nurnberger, C. Schneider, G.V.M. van Osch, C. Keibl, B. Rieder, X. Monforte, A.H. Teuschl, S. Muhleder, W. Holnthoner, B. Schadl, C. Gahleitner, H. Redl, S. Wolbank, Repopulation of an auricular cartilage scaffold, AuriScaff, perforated with an enzyme combination, Acta Biomater. 86 (2019) 207–222, https://doi.org/10.1016/j.actbio.2018.12.035.
[36] P. Li, L. Fu, Z. Liao, Y. Peng, C. Ning, C. Gao, D. Zhang, X. Sui, Y. Lin, S. Liu, C. Hao, Q. Guo, Chitosan hydrogel/3D-printed poly(epsilon-caprolactone) hybrid scaffold containing synovial mesenchymal stem cells for cartilage regeneration based on tetrahedral framework nucleic acid recruitment, Biomaterials 278 (2021) 121131, https://doi.org/10.1016/j.biomaterials.2021.121131.
[37] W. Chen, Y. Xu, Y. Li, L. Jia, X. Mo, G. Jiang, G. Zhou, 3D printing electrospinning fiber-reinforced decellularized extracellular matrix for cartilage regeneration, Chem. Eng. J. 382 (2020) 122986, https://doi.org/10.1016/j.cej.2019.122986.
[38] L. Zhang, Y. Chi, Y. Wei, W. Zhang, F. Wang, L. Zhang, L. Zou, B. Song, X. Zhao, Z. Han, Bone marrow-derived mesenchymal stem/stromal cells in patients with acute myeloid leukemia reveal transcriptome alterations and deficiency in cellular vitality, Stem Cell Res. Ther. 12 (1) (2021) 365, https://doi.org/10.1186/s13287-021-02444-0.
[39] W. Chen, Y. Sun, X. Gu, J. Cai, X. Liu, X. Zhang, J. Chen, Y. Hao, S. Chen, Conditioned medium of human bone marrow-derived stem cells promotes tendon-bone healing of the rotator cuff in a rat model, Biomaterials 271 (2021) 120714, https://doi.org/10.1016/j.biomaterials.2021.120714.
[40] Y. Xu, J. Dai, X. Zhu, R. Cao, N. Song, M. Liu, X. Liu, J. Zhu, F. Pan, L. Qin, G. Jiang, H. Wang, Y. Yang, Biomimetic trachea engineering via a modular ring strategy based on bone-marrow stem cells and atelocollagen for use in extensive tracheal reconstruction, Adv. Mater. (2021), e2106755, https://doi.org/10.1002/adma.202106755.
[41] F. Xu, Q. Zhang, H. Wang, Establishing a density-based method to separate proliferating and senescent cells from bone marrow stromal cells, Aging (Albany NY) 12 (14) (2020) 15050–15057, https://doi.org/10.18632/aging.103569.
[42] C. Posel, K. Moller, W. Frohlich, I. Schulz, J. Boltze, D.C. Wagner, Density gradient centrifugation compromises bone marrow mononuclear cell yield, PLoS One 7 (12) (2012), e50293, https://doi.org/10.1371/journal.pone.0050293.
[43] W. Changchen, W. Hongquan, Z. Bo, X. Leilei, J. Haiyue, P. Bo, The characterization, cytotoxicity, macrophage response and tissue regeneration of decellularized cartilage in costal cartilage defects, Acta Biomater. 136 (2021) 147–158, https://doi.org/10.1016/j.actbio.2021.09.031.
[44] Q. Yang, J. Peng, Q. Guo, J. Huang, L. Zhang, J. Yao, F. Yang, S. Wang, W. Xu, A. Wang, S. Lu, A cartilage ECM-derived 3-D porous acellular matrix scaffold for in vivo cartilage tissue engineering with PKH26-labeled chondrogenic bone marrow-derived mesenchymal stem cells, Biomaterials 29 (15) (2008) 2378–2387, https://doi.org/10.1016/j.biomaterials.2008.01.037.
[45] Y. Xu, D. Li, Z. Yin, A. He, M. Lin, G. Jiang, X. Song, X. Hu, Y. Liu, J. Wang, X. Wang, L. Duan, G. Zhou, Tissue-engineered trachea regeneration using decellularized trachea matrix treated with laser micropore technique, Acta Biomater. 58 (2017) 113–121, https://doi.org/10.1016/j.actbio.2017.05.010.
[46] X.N. Xiang, S.Y. Zhu, H.C. He, X. Yu, Y. Xu, C.Q. He, Mesenchymal stromal cell-based therapy for cartilage regeneration in knee osteoarthritis, Stem Cell Res. Ther. 13 (1) (2022) 14, https://doi.org/10.1186/s13287-021-02689-9.
[47] S. Wang, L. Yang, B. Cai, F. Liu, Y. Hou, H. Zheng, F. Cheng, H. Zhang, L. Wang, X. Wang, Q. Lv, L. Kong, K.B. Lee, Q. Zhang, Injectable hybrid inorganic nanoscaffold as rapid stem cell assembly template for cartilage repair, Natl. Sci. Rev. 9 (4) (2022) nwac037, https://doi.org/10.1093/nsr/nwac037.
[48] Y. Nishida, Y. Hashimoto, K. Orita, K. Nishino, T. Kinoshita, H. Nakamura, Intra-articular injection of stromal cell-derived factor 1alpha promotes meniscal healing via macrophage and mesenchymal stem cell accumulation in a rat meniscal defect model, Int. J. Mol. Sci. 21 (15) (2020), https://doi.org/10.3390/ijms21155454.
[49] R. Bragg, W. Gilbert, A.M. Elmansi, C.M. Isales, M.W. Hamrick, W.D. Hill, S. Fulzele, Stromal cell-derived factor-1 as a potential therapeutic target for osteoarthritis and rheumatoid arthritis, Ther. Adv. Chronic Dis. 10 (2019), https://doi.org/10.1177/2040622319882531, 2040622319882531.
[50] X. Wu, M. Zhou, F. Jiang, S. Yin, S. Lin, G. Yang, Y. Lu, W. Zhang, X. Jiang, Marginal sealing around integral bilayer scaffolds for repairing osteochondral defects based on photocurable silk hydrogels, Bioact. Mater. 6 (11) (2021) 3976–3986, https://doi.org/10.1016/j.bioactmat.2021.04.005.
[51] Y. Sun, Y. You, W. Jiang, B. Wang, Q. Wu, K. Dai, 3D bioprinting dual-factor releasing and gradient-structured constructs ready to implant for anisotropic cartilage regeneration, Sci. Adv. 6 (37) (2020), https://doi.org/10.1126/sciadv.aay1422.
[52] K.L. Spiller, Y. Liu, J.L. Holloway, S.A. Maher, Y. Cao, W. Liu, G. Zhou, A.M. Lowman, A novel method for the direct fabrication of growth factor-loaded microspheres within porous nondegradable hydrogels: controlled release for cartilage tissue engineering, J. Contr. Release 157 (1) (2012) 39–45, https://doi.org/10.1016/j.jconrel.2011.09.057.
[53] L. Uebersax, H.P. Merkle, L. Meinel, Insulin-like growth factor I releasing silk fibroin scaffolds induce chondrogenic differentiation of human mesenchymal stem cells, J. Contr. Release 127 (1) (2008) 12–21, https://doi.org/10.1016/j.jconrel.2007.11.006.
[54] M. Zheng, Stem cells promote the regeneration of knee joint degenerative bone and articular cartilage, J. Healthc Eng. 2022 (2022) 9533211, https://doi.org/10.1155/2022/9533211.
[55] C.H. Chang, T.F. Kuo, C.C. Lin, C.H. Chou, K.H. Chen, F.H. Lin, H.C. Liu, Tissue engineering-based cartilage repair with allogenous chondrocytes and gelatin-chondroitin-hyaluronan tri-copolymer scaffold: a porcine model assessed at 18, 24, and 36 weeks, Biomaterials 27 (9) (2006) 1876–1888, https://doi.org/10.1016/j.biomaterials.2005.10.014.
[56] Z. Wang, H. Le, Y. Wang, H. Liu, Z. Li, X. Yang, C. Wang, J. Ding, X. Chen, Instructive cartilage regeneration modalities with advanced therapeutic implantations under abnormal conditions, Bioact. Mater. 11 (2022) 317–338, https://doi.org/10.1016/j.bioactmat.2021.10.002.
[57] L. Jia, Y. Hua, J. Zeng, W. Liu, D. Wang, G. Zhou, X. Liu, H. Jiang, Bioprinting and regeneration of auricular cartilage using a bioactive bioink based on microporous photocrosslinkable acellular cartilage matrix, Bioact. Mater. 16 (2022) 66–81, https://doi.org/10.1016/j.bioactmat.2022.02.032.